Source Apportionment and Evolution of N-containing Aerosols at a Rural Cloud Forest in Taiwan by Isotope Analysis

Ting-Yu Chen[1], Chia-Li Chen[1], Yi-Chi Chen[2], Charles C.-K. Chou[3], Haojia Ren[*,2], and Hui-Ming Hung[*,1]

[1]Department of Atmospheric Sciences, National Taiwan University, Taipei, 10617 Taiwan
[2]Department of Geosciences, National Taiwan University, Taipei, 10617 Taiwan
[3]Research Center of Environmental Changes, Academia Sinica, Taipei, 11529 Taiwan

Correspondence to: Hui-Ming Hung (hmhung@ntu.edu.tw) and Haojia Ren (abbyren@ntu.edu.tw)

Abstract. Ammonium and nitrate are major N-containing aerosol components. The deposition of N-containing aerosols has impacts on regional ecology and the biogeochemical cycle. In this study, aerosols in a rural cloud forest (Xitou in Taiwan) were studied using ^{15}N and ^{18}O isotope analysis to assess the sources and formation pathways of the local N-containing aerosols linking to a metropolitan. Aerosol samples of different size ranges were collected using a micro-orifice uniform deposit impactor (MOUDI) on a half-day basis in December 2018. The chemical functional groups were analyzed using a Fourier transformed infrared spectroscopy with attenuated total reflection technique (FTIR-ATR), while the isotope analysis was performed using a gas chromatography-isotope ratio mass spectrometer (GC-IRMS). The average measured aerosol concentration (PM_{10}) was 0.98 (ranging from 0.15 to 3.31) and 0.25 (ranging from 0.00 to 1.51) $\mu g/m^3$ for NH_4^+ and NO_3^-, respectively. In general, a higher concentration was observed during the daytime by a factor of 1.5 to 6 than nighttime, likely due to the transportation of pollutants from upper stream urban and industrial regions through the local sea breeze combined with valley wind. The presence of fog can further elevate the concentration by a factor of 2 to 3, resulting from the stronger inversion and lower boundary layer height. The higher NH_4^+ concentration in fine particles under foggy conditions corresponds to submicron-sized NO_3^- formation via aqueous phase dissolution with NH_4^+ neutralization. Furthermore, the higher RH during fog events shifted the mass distribution of aerosol functional groups to a larger mode size. By comparing the $\delta^{15}N$ value directly or through the analysis using a statistical isotope mixing model, MixSIAR, NH_4^+ is probably originated from the industries, coal-fired power plants (CFPP), or fertilizer plants, while NO_3^- might be contributed from the CFPP, industrial or urban sources. The overall $\delta^{18}O$ of NO_3^- is +72.66‰ ± 3.42‰, similar to that in other winter Asia studies, suggesting the major formation pathway via O_3 oxidation ($\delta^{18}O$ = +72.5 to 101.67‰). However, a lower $\delta^{18}O$ (< +67‰) for particles less than 0.56 µm during foggy daytime suggests the local contribution via the peroxyl radical oxidation before partitioning into aerosol phase under foggy conditions. Overall, the $\delta^{15}N$ and $\delta^{18}O$ distribution profiles as a function of particle size in the studied rural forest site reveal the evolution of aerosol composition from remote coastal regions with chemical processes along the transport process, which can be further affected by weather conditions such as fog events.

Keywords: aerosol, fog, functional group, nitrogen isotope, oxygen isotope

1 Introduction

Aerosols play an essential role in weather, climate, ecology, and human health (Poschl, 2005; Seinfeld and Pandis, 2006) and are mainly composed of sulfate, nitrate, ammonium, and other organic species. Nitrogen is one of the significant elements of aerosol in various forms, such as ammonium, nitrate, organic nitrogen, etc. Ammonium and nitrate are the primary N-containing cation and anion species, respectively, and the balance of the ions can influence aerosol acidity. Also, the local weather, such as fog formation, can be affected by the aerosol characteristics via the hygroscopicity of aerosols (Petters and Kreidenweis, 2007). Furthermore, the N-containing aerosols not only affect human health and climate but also play an important role in the regional and global nitrogen biogeochemical cycles. The long-range transport of N-containing aerosols from human activities may result in additional nutrient input at deposition sites, affecting local plant growth and ecology (Bobbink et al., 2010). Therefore, the amount of the N-containing aerosols formed and transported to the rural area and their potential sources should be investigated to evaluate the origin of the N-containing species and their impacts.

Ammonium in aerosols could form from gaseous ammonia, mainly generated from agricultural activities (Behera et al., 2013). Besides, NH_3 from fossil fuel exhaust and slipping during selective catalytic reduction (SCR) processes also contribute to aerosol NH_4^+ formation (Cape et al., 2004). Nitrate in aerosols is produced by oxidation of its precursors, nitrogen oxides (NO_x), emitted from fossil fuel combustion, biomass burning, lightening, and biogenic soil emission. The formation pathway of aerosol NO_3^- varies with conditions. In the daytime, NO can be oxidized by O_3 or peroxyl radicals to form NO_2, which could be photolyzed back to NO or further react with OH radicals to generate nitric acid, forming the nitrate aerosols. At night, NO_2 may further be oxidized to NO_3, reacting with other NO_2 to form N_2O_5. The hydrolysis of N_2O_5 gives another pathway to form nitrate aerosols (Jacob, 1999; Seinfeld and Pandis, 2006).

The stable nitrogen isotope in aerosols provides a clue about the probable sources of nitrogen content. Since the abundance of ^{15}N and ^{14}N in gaseous precursors of NH_4^+ and NO_3^- varies in different emission sources, the $\delta^{15}N$, defined as $((^{15}N/^{14}N)_{sample}/(^{15}N/^{14}N)_{air} - 1) \times 1000$ (‰), can act as an indicator of the associated nitrogen species (Felix et al., 2012; Felix et al., 2014; Walters et al., 2015; Pan et al., 2016; Chang et al., 2016; Savard et al., 2017; Pan et al., 2018a; Zhang et al., 2020). For nitrate, not only the $\delta^{15}N$ can be an index of sources, but the $\delta^{18}O$, defined as $((^{18}O/^{16}O)_{sample}/(^{18}O/^{16}O)_{VSMOW} - 1) \times 1000$ (‰), where VSMOW stands for Vienna Standard Mean Ocean Water, can reveal the oxidation pathway (Fig. 1) of nitrate formation due to the $\delta^{18}O$ difference between its oxidants: O_3, OH, RO_2 (including hydrogen peroxyl and organic peroxyl radicals), and H_2O (Hastings et al., 2003; Fang et al., 2011; Gobel et al., 2013).

Xitou, an experimental forest of National Taiwan University, is a planted forest located in central Taiwan. As the origin of Beishih brook, Xitou is in the position of a river valley topography towards the northwest, connecting to Taichung City Metropolitan. Due to the topography, the sea breeze combined with mountain-valley wind dominates the diurnal local circulation, bringing air mass from different regions between daytime and nighttime. During the daytime, the sea breeze combined with valley wind can bring pollutants along the transporting path from coastal areas passing through the coal-fired power plants, industrial sites, and cities. As the wind direction reverses during nighttime, the pollutant concentration decreases

65 (Chen et al., 2021). Besides, the afternoon upslope fog occurs frequently in the Xitou forest due to the boundary layer inversion and the sea breeze combined with valley wind (Hsieh, 2019). Therefore, the fog might affect aqueous chemical processes locally.

The analysis of $\delta^{15}N$ and $\delta^{18}O$ for nitrogen-associated species as a function of particle size might provide the origin of the N-containing species and the evolution of transport and chemical processes. This study aims to investigate: 1) the interaction

70 between local circulation and the aerosol composition in a rural forest area linking to a city, 2) how the weather affects the aerosol composition in different sizes, and 3) the source apportionment of rural N-containing aerosols by isotopic analysis.

2 Experiment Setup

A field campaign was conducted over Xitou experimental forest (23°40'12" N, 120°47'54'' E, 1,179 m a.s.l.) in a valley from 1st to 24th December 2018 to investigate the interaction between air quality, local circulation, and human activities in central

75 Taiwan. To dig into the link between local circulation and aerosol concentration and composition, aerosol samples in different sizes were collected separately for daytime and nighttime using a cascade impactor, and underwent Fourier transformed infrared spectroscopy (FTIR) analysis for the functional group concentration (Coury and Dillner, 2008; Hung et al., 2016). Furthermore, $\delta^{15}N$ and $\delta^{18}O$ of N-containing species were measured using the denitrifier method (Sigman et al., 2001; Casciotti et al., 2002). The period mass-averaged $\delta^{15}N$ values were further analyzed using a mixed stable isotope analysis in R package

80 (MixSIAR) (Stock et al., 2018) to resolve the potential sources of aerosol, while $\delta^{18}O$ acts as an indicator of the oxidation pathway for nitrate formation in aerosols.

2.1 Sample collection

Ambient aerosol samples were collected using a 13-stage MOUDI (micro-orifice uniform deposit impactors, Model 125R, MSP Corporation, Shoreview, Minnesota, USA) with 46.2 mm polytetrafluoroethylene (PTFE) membrane filters (Whatman

85 7592-104). The cut-off size of MOUDI was 0.01, 0.018, 0.032, 0.056, 0.1, 0.18, 0.32, 0.56, 1.0, 1.8, 3.2, 5.6 and 10 μm, respectively, and the flow rate of sampling air was 10 L min^{-1}. The samples were categorized into daytime and nighttime to investigate the impact of daily mountain/valley-breeze circulation on aerosols. Daytime samples were collected from ~9:00 to ~17:00 (local time), and nighttime samples were from ~18:00 to ~6:00 the next day to represent the valley and mountain breeze, respectively. 20 sets of filter samples were collected from 2nd December 2018 to 22nd December 2018, including 4

90 foggy samples (181207D, 181213N, 181214D, 181215D, YYMMDD Daytime/Nighttime) and 16 non-foggy samples (181202D/N, 181207N, 181208D/N, 181209D/N, 181214N, 181215N, 181216D/N, 181220N, 181221D/N, 181222D/N). The collected filter samples were sealed, covered by aluminum foil, and preserved under 4°C till the laboratory analysis to prevent contamination.

2.2 FTIR-ATR Analysis

95 The concentrations of functional groups such as NH_4^+, NO_3^- and SO_4^{2-} were determined via FTIR measurement (Nicolet 6700, Thermo Fisher Scientific, USA) equipped with a single-reflectance attenuated total reflectance (ATR) monolithic diamond accessory (GladiATR™, PIKE Technologies, USA). Filter samples were pressure-pressed onto the ATR crystal to ensure a closed contact with the crystal. The infrared spectra were scanned at wavenumbers from 4000 to 500 cm^{-1} with a resolution of 1 cm^{-1}. The selected spectrum for a given wavenumber range was fitted with one or multiple Lorentzian curves to derive the

100 peak absorbance (I) of each functional group as shown in Fig. S1. The curve fitting function can be written as follows:

$$A(\nu) = I \times \frac{\sigma^2}{4(\nu - \nu_{peak})^2 + \sigma^2} \tag{1}$$

where $A(\nu)$ is the distribution of a specific absorption curve as a function of wavenumber (ν), and σ is the scale parameter (half-width at half-maximum) associated with the width of the absorption curve. For a mixture, the observed spectrum is a superposition of each substance i:

105 $$A\left(\nu, \left(\nu_{peak,1}, \sigma_1, I_1\right), \left(\nu_{peaki2}, \sigma_2, I_2\right), \dots \right) = \sum_i A_i(\nu) = \sum_i I_i \times \frac{\sigma_i^2}{4(\nu - \nu_{peak,i})^2 + \sigma_i^2} \tag{2}$$

The fitted peaks includes ~1350 cm^{-1} for nitrate and ~1417 cm^{-1} for ammonium (Fig. S2); besides, the absorbance peak at ~1080 cm^{-1} for SO_4^{2-} was applied in a 3-curve fitting to differentiate the contribution by the nearby absorbance of the PTFE filter (Fig. S3). Therefore, the calibration of absorbance to concentration was based on the previous analysis using the correlation of absorbance of FTIR functional groups to the water-soluble ions measured by ion chromatography (Huang, 2016).

110 As to black carbon (BC) concentration, the absolute absorbance at 3950 ± 5 cm^{-1} is applied to quantify the BC concentration based on the calibration done by Huang (2016) with the elemental carbon concentration determined using a DRI2001A carbonaceous aerosol analyzer, following the IMPROVE thermo-optical reflectance (TOR) protocol (Chow et al., 2001), as detailed in Chou et al. (2010).

2.3 Isotope Analysis

2.3.1 Sample Analysis

115

The isotope analysis requires at least five nmol of equivalent N in 5mL solution (i.e., the molar concentration of $NO_3 + NH_4 \geq$ 1μM N) so the FTIR measurements provide a quantitative reference to infer the concentration of dissolved N-containing species. 10 sets of aerosol samples with higher N-containing functional group concentration under distinct weather conditions were selected for $\delta^{15}N$ and $\delta^{18}O$ isotope analysis of N-containing species (181202D/N, 181213N, 181214D/N, 181215D,

120 181220N, 181221D, 181222D, 181222N). If the predicted concentration of one filter was too low, 2 to 4 filters collected on the same day with adjacent size bins were put together in a bottle during the rinsing process to ensure sufficient concentration for isotope analysis. Filter samples were cut in half and soaked into 30 mL Milli-Q water (resistivity = 18.2 MΩ at 25 °C) and underwent a 30-minute ultrasonication to dissolve the water-soluble ions into the solution. Afterward, the extracted solution

was filtered through a 0.22 μm Millipore syringe filter and then preserved in an HDPE bottle. The samples were analyzed for

125 the $\delta^{15}N$ of total nitrogen (TN) and nitrate + nitrite (NN), and the $\delta^{18}O$ of NN by the bacterial "denitrifier method" as stated by Sigman et al. (2001), Casciotti et al. (2002), and updated by Weigand et al. (2016). For TN analysis, the oxidation process by adding potassium persulfate in NaOH solution was to oxidize NH_4^+ and other N-containing species in a reduced state into NO_3^- before bacterial digestion. The isotope $^{15}N/^{14}N$ and $^{18}O/^{16}O$ was measured using a gas chromatography-isotope ratio mass spectrometer (GC-IRMS) composed of a GC column system coupled with Thermo MAT 253 Plus 10 kV IRMS. The

130 international standard IAEA-NO3 ($\delta^{15}N$ = 4.7 ‰, $\delta^{18}O$ = +25.61‰) and USGS 34 ($\delta^{15}N$ = -1.8 ‰, $\delta^{18}O$ = -27.93 ‰) were applied for $\delta^{15}N$ and $\delta^{18}O$ calibration (Bohlke et al., 2003). In each batch of measurement, three to five duplicates of standards and bacteria blank were used to ensure the efficiency of bacterial conversion and the stability of mass spectroscopy. The detail of isotope ratio measurement is described in the supplementary material.

Ammonium is a major N-containing component in aerosols as part of TN. Since the concentration of water-soluble TN minus

135 NN correlates well (R^2=0.7764) with the measured NH_4^+ concentration from FTIR (slope is close to 1 with a small interception as shown in Fig. S4), the water-soluble TN-NN can seem as NH_4^+. Therefore, the $\delta^{15}N$ of ammonium can be derived by assuming the collected aerosol mainly comprised of nitrate, nitrite, and ammonium with negligible other N forms such as organic nitrogen (Wu et al., 2021). The $\delta^{15}N$ of NH_4^+ can be calculated using Eq. (3) as follows:

$$\delta^{15}N_{NH_4^+} = \frac{\delta^{15}N_{TN} \times M_{TN} - \delta^{15}N_{NN} \times M_{NN}}{M_{TN} - M_{NN}} \tag{3}$$

140 where M_{TN} and M_{NN} are the molarities of total nitrogen (TN) and nitrate plus nitrite (NN) of the sample solution, respectively. If organic nitrogen is considered, a slightly higher $\delta^{15}N$ of NH_4^+ than the current reported values can be expected because organic nitrogen might be related to NO_x and was reported a lower $\delta^{15}N$ ($\leq$ -5‰) than nitrate (Wu et al., 2021). Additionally, since the aerosol nitrite concentration is mostly negligible based on ion-chromatography (IC) analysis of PM_{10}, NN is assumed to be in NO_3^- form, i.e., $\delta^{15}N$ of $NO_3^- \approx \delta^{15}N_{NN}$.

145 **2.3.2 Bayesian Mixing Model Application**

A Bayesian mixing model, MixSIAR, was applied to assess the contribution of multiple aerosol sources. MixSIAR is a statistical model applying Bayesian Inference to infer the posterior probability of mixture sources by analyzing its tracer composition, such as stable isotope or fatty acids (Stock et al., 2018). The studied tracers are assumed to transfer from sources to the mixture through a conserved mixing process integrating the observed variability. In this study, the observed mass-

150 weighted $\delta^{15}N$ of NH_4^+ and NO_3^- for each sampling period was used as prior information of the mixture. For simplification, the source data adopted the results of Savard et al. (2017) as summarized in Table 1 by assuming that the $\delta^{15}N$ of NH_4^+ and NO_3^- was directly related to their emission sources, either single source or mixture from those sources. The source data for MixSIAR analysis include $\delta^{15}N$ of NH_4^+ from traffic, chemical and metal industries, feedlots, fertilizer plants, and coal-fired power plants (CFPP), and $\delta^{15}N$ of NO_3^- from traffic, chemical and metal industries, fertilizer plants and oil refinery, and CFPP.

155 The gas compressors source was not considered in this study.

3 Results and Discussion

3.1 Functional group concentration by FTIR-ATR

The averaged functional group concentration measured using FTIR-ATR of collected 0.01 to 10 μm samples was NH_4^+: 0.98 μg/m^3, NO_3^-: 0.25 μg/m^3, SO_4^{2-}: 5.16 μg/m^3, and black carbon (BC): 0.81 μg/m^3 as summarized in Table 1. The mass
160 concentration distribution of NH_4^+ and NO_3^- as a function of aerosol size is shown in Fig. 2. NH_4^+ is mainly distributed in submicron mode, with the most significant mass concentration in 0.32-0.56 μm size bin. The NO_3^- during the non-foggy period mostly appears in sizes larger than 1 μm and peaks at 3.2-5.6 μm. The mass distribution pattern of SO_4^{2-} mainly in the sub-micron mode is consistent with that of NH_4^+ (Fig. S5), which suggests that most ammonium is in the form of sulfate-associated salts. On the contrary, NO_3^- in the aerosol is formed from the substitution reaction of sea salt aerosol or dust in the larger size
165 (> 1 μm) aerosols by HNO_3 (Evans et al., 2004). The non-observed nitrate in submicron particles during non-foggy days is likely due to the thermodynamic equilibrium under ammonia-limited conditions (Seinfeld and Pandis, 2006). Generally, the concentration during daytime was higher than that at nighttime (Table 1). Foggy weather also promoted a higher concentration with further discussion in the following subsections.

3.1.1 Difference between daytime and nighttime

170 The functional group concentration of NH_4^+ (1.00 μg/m^3) and NO_3^- (0.25 μg/m^3) during non-foggy daytime was higher than that in non-foggy nighttime (0.56 μg/m^3 and 0.04 μg/m^3, respectively) as shown in Table 1, and SO_4^{2-} and BC also have approximately 1.5 times higher concentration during non-foggy daytime. The greater daytime concentration might link to the upstream transportation of urban pollutants by valley wind combined with the sea breeze (Chen et al., 2021). The sampling site is mostly below the boundary layer height during daytime and above the boundary layer height during nighttime. Once the
175 wind direction changes into mountain wind accompanying land breeze, the cleaner upper-stream air dilutes the pollutants in the Xitou Forest area.

3.1.2 The Influence of Fog

The daytime concentration of NH_4^+ and NO_3^- was 2 to 4 times higher in the foggy period than that in the non-foggy period (Table 1). The mass distribution seems to shift to a larger size bin (0.56-1.8μm) for NH_4^+ as shown in Fig. 2(c), while NO_3^- in
180 Fig. 2(d) also has a significantly high concentration for the 0.56-1.8μm size bin during the foggy period. Higher ammonium nitrate concentration might result from the stronger boundary layer inversion on foggy days. When the boundary inversion gets stronger in Xitou area, the moisture transportation by upwelling turbulence is weakened. Therefore, water vapor could accumulate in the lower atmosphere, promoting fog formation and prolonging fog lifetime (Hsieh, 2019). Furthermore, the weakened upward transport could also accumulate pollutants in the lower boundary layer, causing a higher observed
185 concentration. The enhanced concentration of black carbon (BC), a primary aerosol component with limited chemical reactions

in the atmosphere, during foggy periods (Table 1 and Fig. S5) can further reveal the inference of the boundary layer on aerosol concentration.

The observed mass distribution of NH_4^+ shifting slightly to a larger size mode on foggy days is likely due to the hygroscopic growth of aerosols. According to a previous calculation with the observed dry and wet aerosol size distribution in Xitou, NH_4^+-containing aerosol has a hygroscopicity parameter of 0.21±0.01 (Chen et al., 2021). The hygroscopic growth of aerosol from averaged RH of 80% under non-foggy circumstances to over 99% during the foggy period could lead to a larger wet aerosol size. Extra high NO_3^- concentration of 0.56-1 μm aerosol was observed during foggy periods accompanied by the high NH_4^+ concentration in that size bin (Fig. 2(d)). In foggy periods, the higher water content of aerosol promotes an aqueous phase reaction of HNO_3 uptake on aerosols, and the higher concentration of NH_4^+, more than $2\times[SO_4^{2-}]$, gives extra neutralizing cation to stabilize the NO_3^- as suggested by Chen et al. (2021).

3.2 Isotope Analysis of N-containing species

The $\delta^{15}N$ of NH_4^+ and NO_3^- discussed in this section infers the probable aerosol sources, while the measured $\delta^{18}O$ of NO_3^- infers the photo-oxidation processes of NO_x. The isotope value of each sample is shown in Fig. 3, and the period mass-weighted averaged $\delta^{15}N$ and $\delta^{18}O$ are summarized in Figure 4 and Table S1.

3.2.1 $\delta^{15}N$ of NH_4^+

Figure 3(a) shows the $\delta^{15}N$ value of aerosol NH_4^+ as a function of geometric averaged particle diameter. The $\delta^{15}N$ varies from -3.70‰ to +21.39‰, and the average mass-weighted $\delta^{15}N$ value is +11.95‰ with a standard deviation of 2.65‰. The $\delta^{15}N$ of 0.32-1 μm aerosols is in the range of +7.16‰ to +18.64‰, relatively higher than that of the larger and smaller size bins. The increasing and then decreasing trend of NH_4^+ $\delta^{15}N$ with aerosol size was also observed in Beijing (Pan et al., 2016; Pan et al., 2018b) but was approximately 12‰ lower. This offset probably results from the different emission sources or the partitioning processes. Overall, the processes forming aerosol NH_4^+ may lead to the size differentiated $\delta^{15}N$.

The daytime $\delta^{15}N$ of NH_4^+ is mostly greater than the nighttime one as summarized in Table 3, likely resulting from the different sources, such as transportation of high-$\delta^{15}N$ NH_3 from urban rush-hours traffic or industrial sources by sea breeze combined with the valley wind. As the mountain wind dominates after sunset, available NH_3 might be attributed to the daytime residual (having lower $\delta^{15}N$ due to the fractionation that happened during daytime) or the local biogenic sources having a lower $\delta^{15}N$. Fog varies the mass size distribution among components and can affect the isotopic ratio. Under foggy daytime conditions, the $\delta^{15}N$ value of larger size aerosols (PM_{1-10}-NH_4^+) was more likely to be the extension of 0.56-1 μm with a value up to 21.39‰, higher than that of non-foggy days. As stated in section 3.1, high NH_3 concentration can promote the partition of HNO_3 under foggy condition. The observed flat trend of $\delta^{15}N$ at diameter $\geq$ 0.56 μm might result from the hygroscopic particle growth of NH_4^+ from the 0.56-1 μm size bin aerosols. As NH_4^+ is likely to deliquesce to the liquid phase under high RH conditions, the gas-liquid phase transition could accompany isotope equilibrium fractionation for most aqueous particles (Walters et al., 2018). The NH_3-rich and high RH conditions might cause the NH_3 partition to condensed phase and favor higher $\delta^{15}N$ during

equilibrium fractionation processes (Pan et al., 2018b). On non-foggy days, having a relatively lower concentration with more acidic properties (indicating NH_3 limited), a higher portion of NH_3 might participate in the aerosol phase to lead to a lower $\delta^{15}N-NH_4^+$ toward the original $\delta^{15}N-NH_3$.

3.2.2 $\delta^{15}N$ of NO_3^-

The $\delta^{15}N$ value of NO_3^- as a function of size bin shown in Fig. 3(b) ranges from -1.07 to +6.64‰, with a mass-weighted mean value of +2.98‰ and a standard deviation of 1.20‰. This value agrees with other studies measured in Asia or the Pacific Ocean in winter to spring period (-1‰ ± 3‰ in spring by Guha et al. (2017); 2.0‰ ± 0.4‰ in spring and 8.6‰ ± 0.4‰ in winter by Kim et al. (2019); 3.1 ± 1.1 ‰ in winter by Kawashima (2019)). As stated in section 3.1.2., nitrate significantly contributes to the submicrometer particles during foggy daytime in addition to the usual peak over the supermicrometer particles for all conditions (Fig. 2). The nitrate can be divided into two groups, $PM_{1-10}-NO_3^-$ for particle size in the range of 1 to 10 μm and $PM_1-NO_3^-$ for particle diameter less than 1 μm, for further discussion. For a given sampling period, $PM_1-NO_3^-$ has lower $\delta^{15}N$ (-1.07 to +3.19‰) than $PM_{1-10}-NO_3^-$ (+1.85 and +6.64‰), likely due to different formation processes. $PM_{1-10}-NO_3^-$ might be formed through the reaction of HNO_3 or NO_2 with the coarse particles composing NaCl or dust (Evans et al., 2004; Hoffman et al., 2004) during the transport from the coast through the urban region and further to Xitou. Therefore, a higher $\delta^{15}N$ NO_3^- participates in the aerosol-phase through isotopic equilibrium fractionation with lower $\delta^{15}N$ $HNO_{3(g)}$ or NO_2 gas molecules remaining in the air (Walters and Michalski, 2015). In contrast, $PM_1-NO_3^-$ occurs only on foggy days, probably forming in the mountain region with high water content and available NH_3. The available $HNO_{3(g)}$ for PM_1 is from the residual NO_x (after reacting with coarse mode particles at the upper stream) and has lower $\delta^{15}N$ than $PM_{1-10}-NO_3^-$. The $PM_1-NO_3^-$ formed through the aqueous phase reaction under high NH_4^+ with effective gas-phase HNO_3 uptake might have a limited isotopic selection leading to a low $\delta^{15}N$ of NO_3^- under foggy conditions.

The sample of 21D is a special case with higher $\delta^{15}N$ values. It might result from the recorded agricultural activities nearby, including fertilizing and mowing. The fertilizer generates NO_x with higher $\delta^{15}N$ (Savard et al., 2017), which indicates that the agricultural activities might cause higher $\delta^{15}N$ values than on other days.

3.2.3 $\delta^{18}O$ of NO_3^-

The $\delta^{18}O$ of NO_3^- ranged from +53.90 to +79.81‰ (Fig. 3(c)), with a half-day period mass-weighted average of +72.66‰ and a standard deviation of 3.42‰. The results are within the observed $\delta^{18}O$ range in cool seasons over Mt. Lulin site in Taiwan (69‰ ± 15‰ reported by Guha et al. (2017)) and in the typical range of other studies (averaged value from 70.9‰ to 83.8 ‰) (Savarino et al., 2007; Wankel et al., 2010; Fan et al., 2020; Sun et al., 2020). The relatively higher $\delta^{18}O$ compared to summer samples (32 ± 13‰ reported by Guha et al. (2017)) indicates that more NO_3^- precursors (i.e., NO_x) were formed by O_3 oxidation whether it was further oxidized through OH oxidation of NO_2 or N_2O_5 hydrolysis pathways (from +72.5‰ to +101.67‰, detailed in SI description). The slightly lower daytime $\delta^{18}O$ (+69.67‰ to +72.52‰ based on half-day average) compared to nighttime samples (+74.82‰ to +79.81‰) as shown in Table S1 indicates that peroxyl radicals might partially participate in

the daytime photooxidation processes or relatively lower $\delta^{18}O$ of OH leading to a lower $\delta^{18}O$ in nitrate aerosols during daytime as stated in other studies (Gobel et al., 2013; Hastings et al., 2003; Fang et al., 2011).

For PM_1, the $\delta^{18}O$ of 0.32-0.56 μm NO_3^- under foggy conditions (+53.90‰ and +66.13‰ for 14th December and 15th December daytime sample, respectively) is relatively lower than that over larger sizes (e.g., +75.65‰ and +73.98‰ of 0.56-1 μm) suggesting the formation pathway difference. The concentration of 0.32-0.56 μm NO_3^- is relatively lower than that of 0.56-1 μm or PM_{1-10}, and it might attribute to ambient air mass nearby the observation site. Because the fine particles are more acidic (Chen et al., 2021), NO_3^- can frequently exchange with gas-phase HNO_3 to reveal the local $\delta^{18}O$ of NO_3^-. The peroxyl radicals derived from the biogenic volatile organic compounds photooxidation at Xitou forest area might be active oxidants locally for fine mode organic nitrate ($RONO_2$ or $ROONO_2$) and HNO_3 from $NO + RO_2 \rightarrow NO_2 + RO$ and $NO_2 + OH \rightarrow HNO_3$ oxidation to have a lower $\delta^{18}O$ of NO_3^- (SI description). On the other hand, the higher $\delta^{18}O$ of 0.56-1 μm NO_3^- is likely formed from the growth of smaller particles and aqueous phase reactions such as HNO_3 partition, which could be neutralized by excess NH_4^+ at an earlier stage to be less influenced by peroxyl radicals. Furthermore, the PM_{1-10}-NO_3^- are mainly produced nearby the urban regions via the reactions of HNO_3 or NO_x with sea salt, i.e., $HNO_3 + NaCl_{(p)} \rightarrow HCl_{(g)} + NaNO_{3(p)}$ or $2NO_2 + NaX_{(p)} \rightarrow XNO_{(g)} + NaNO_{3(p)}$ (X = Cl or Br, (p) represents particle phase), which may also produce NO_3^- with a higher $\delta^{18}O$ because most O atoms of NO_3^- might be from O_3 during the fast $NO \leftrightarrow NO_2$ conversion processes (Gobel et al., 2013).

3.3 Source apportionment by isotope analysis

The $\delta^{15}N$ of collected NH_4^+ and NO_3^- is applied for source apportionment since $\delta^{15}N$ in N-containing aerosol is dependent on the precursor sources (Felix and Elliott, 2014; Walters et al., 2015; Chang et al., 2016; Pan et al., 2016; Savard et al., 2017; Pan et al., 2018b; Fan et al., 2019). Figure 4 shows the averaged $\delta^{15}N$ under distinct weather conditions and the isotope value of single-source based on the observation by Sarvard et al. (2017). By assuming that the mass-weighted average isotope represents the possible source contribution with a single source having similar $\delta^{15}N$ as reported by Sarvard et al. (2017) for simplification, the probable aerosol-N sources are summarized in Table 3. Due to the similar $\delta^{15}N$ among sources, NH_4^+ might be originated from several sources such as CFPP, traffic, or industries, but least likely from feedlots. The urban sources or CFPP might contribute to PM_{1-10}-NO_3^-, while industries to the lower $\delta^{15}N$ of PM_1-NO_3^- under foggy conditions. In contrast, the significant difference of $\delta^{15}N$ between measurement and fertilizer plants (+10.8‰) suggests the limited contribution of fertilizer production-related NO_3^-. Overall, the probable sources of NH_4^+ and NO_3^- were anthropogenically originated, such as CFPP, industries, and urban traffic. The sea breeze could transport the precursor gases or aerosol phase pollutants from coastal coal-fired power plants, industrial sources, or urban emissions to the forest area by upslope wind (Chen et al., 2021). During the transportation, the chemical reactions might further promote PM formation, having the measured $\delta^{15}N$ of collected samples close to that of the available gas-phase species.

As PM is a mixture attributed from various sources, the mass-weighted average $\delta^{15}N$ of NH_4^+ and NO_3^- was analyzed using the MixSIAR model to distinguish the posterior probability of aerosol sources as summarized in Table 4. The daytime samples of 21st December were excluded in this analysis due to the interference from the agricultural activities nearby. The similar

posterior probabilities among some sources are due to the comparable source isotope values as stated above. However, with the source and sample variability, the results of MixSIAR provide a broader probability for source contribution and reflect the

285 uncertainty of the ambient conditions simply using the mixing rule. The possible differentiation among the similar $\delta^{15}N$ sources might require the integration of the back trajectory and chemical transport model simulation with the known emission sources. Taking account of all weather conditions, the order of possible sources from the highest to the lowest probability is {industries, CFPP, fertilizers, traffic, feedlots}. The first two sources have a higher likelihood, > 20%. As the conditions were divided by different weather patterns, fertilizer plants have increased the importance, especially for foggy daytime. Feedlots remain the

290 lowest. The model results agree with the direct comparison, indicating that the anthropogenic sources contribute significantly to aerosol-NH_4^+. The larger $\delta^{15}N$ during foggy daytime suggests a higher probability of fertilizer production, indicating the likelihood of locally produced ammonium from the fertilizer manufacturers nearby the agricultural area because of the lower wind speed and lower boundary layer height.

Though the $\delta^{15}N$ of NO_3^- might seem alike (Figure 4), some trends could be revealed from the MixSIAR model analysis. The

295 MixSIAR results show that industries, urban, and CFPP are the major sources for both PM_1-NO_3^- and PM_{1-10}-NO_3^-, whereas fertilizer plants have the lowest probability. The difference in posterior probability between PM_1 and PM_{1-10} nitrate sources is not significant: the PM_{1-10} NO_3^- was more likely from CFPP, industries, or urban sources, while industries had the majority of PM_1-NO_3^- formation. However, the inferred source difference might suggest that the coarse mode aerosols came from the coastal sea salt particles mixing with the emission of coal-fired power plants or the Taichung-Changhua metropolitan during

300 the inland transport. On the other hand, PM_1-NO_3^- is likely formed locally and might have a higher portion of nearby sources. For both PM_1 and PM_{1-10} nitrate, fertilizer industry was the minority in the NO_3^- sources for Xitou forest area, different from the result of NH_4^+. The discrepancy might result from the type of produced nitrogen fertilizers in the nearby area vs. the higher contribution of NO_3^- from the power plant or urban sources through sea breeze and valley wind transport.

4 Conclusions

305 The mass distribution of aerosol NH_4^+ and NO_3^- concentration and the associated isotope analysis were analyzed to investigate the evolution of nitrogen species before reaching the studied site. In Xitou forest, the average concentration of aerosol components is 0.98 $\mu g/m^3$ for NH_4^+ and 0.25 $\mu g/m^3$ for NO_3^-. The 1.5 to 6 times higher concentration of NH_4^+ and NO_3^- in the daytime indicates the local circulation combining land-sea breeze with mountain-valley wind could bring urban and industrial pollutants into the Xitou forests, further proved by the $\delta^{15}N$ analysis. The $\delta^{15}N$ of NH_4^+ from -3.70‰ to +21.39‰ with higher

310 NH_4^+ $\delta^{15}N$ values of the 0.32-1 μm aerosols, where a higher concentration was measured,. The $\delta^{15}N$ of NO_3^- was from -1.07 to +6.64‰, with a mean value of 2.98‰ and a standard deviation of 1.20‰. Though the similar range of NO_3^- among sources made it difficult to distinguish the origin of NO_3^- directly, the statistical model still provided some hints: Industries, urban, and CFPP are the significant sources of particulate NO_3^-. The stronger boundary layer inversion during foggy days led to weaker upward transportation of air mass, causing a 2-3 times higher aerosol concentration. The mass distribution difference and the

315 discrepancy of $\delta^{15}N$ of NO_3^- between foggy and non-foggy conditions suggest that the additional PM_1-NO_3^- for foggy days was formed locally with excess NH_3 in the aqueous phase. The difference in analyzed nitrogen sources between PM_{1-10} and PM_1 NO_3^- revealed the impacts of fog on aerosol formation: PM_{1-10} was more likely produced by CFPP and urban areas, whereas PM_1, existing only in the foggy period, had more local contributors such as a higher portion of industries. The inferred source difference might suggest that the nitrogen atoms of coarse mode aerosols might be formed through the mixing of the

320 coastal sea salt particles with the emission of coal-fired power plants or metropolitan during the inland transport. On the other hand, PM_1-NO_3^- is likely formed locally and might have a higher portion of nitrogen from nearby sources. However, the fractionation during the aerosol transportation under higher RH and high gaseous precursors can enlarge the isotope value in aerosol phases (Chang et al., 2018), which might affect the source apportionment results and should be appropriately assessed in the future. The observed $\delta^{18}O$ of NO_3^- in this study, consistent with former studies conducted in a similar season (Guha et

325 al. 2017), suggests that O_3 is the primary oxidant for NO_x as a precursor of NO_3^-. The lower $\delta^{18}O$ value at 0.32-0.56 μm NO_3^- under foggy daytime conditions indicates the participation of locally produced RO_2 in NO_3^- formation. Overall, the measured composition combined with the weather observation suggests the effects of local circulation and boundary layer on air quality, and the isotope analysis further proved the influence of the inland transport from anthropogenic sources.

Data availability

330 Data are available upon request.

Author contributions

TY Chen and CL Chen carried out the field studies and aerosol composition analysis. TY Chen performed data analysis and MixSIAR model for N source apportionment and prepared the manuscript draft and editing. YC Chen and H Ren developed and conducted the isotope analysis. CCK Chou provides MOUDI instrumentation support and IC analysis of $PM_{2.5}$ and PM_{10}.

335 HM Hung supervised the project, including data discussion and manuscript editing.

Competing interests

The authors declare that they have no conflict of interest.

Acknowledgments

This study is supported by the Ministry of Science and Technology, Taiwan (108-2111-M-002-003, 109-2111-M-002-003, and 110-2111-M-002-010) and National Taiwan University (110L892001). We acknowledge the local site support from the Administration of the Xitou Experimental Forest, College of Bio-Resources and Agriculture at National Taiwan University.

References

Behera, S. N., Sharma, M., Aneja, V. P., and Balasubramanian, R.: Ammonia in the atmosphere: a review on emission sources, atmospheric chemistry and deposition on terrestrial bodies, Environ Sci Pollut Res Int, 20, 8092-8131, 10.1007/s11356-013-2051-9, 2013.

Bobbink, R., Hicks, K., Galloway, J., Spranger, T., Alkemade, R., Ashmore, M., Bustamante, M., Cinderby, S., Davidson, E., Dentener, F., Emmett, B., Erisman, J. W., Fenn, M., Gilliam, F., Nordin, A., Pardo, L., and De Vries, W.: Global assessment of nitrogen deposition effects on terrestrial plant diversity: a synthesis, Ecological Applications, 20, 30-59, 10.1890/08-1140.1, 2010.

Bohlke, J. K., Mroczkowski, S. J., and Coplen, T. B.: Oxygen isotopes in nitrate: new reference materials for 18O:17O:16O measurements and observations on nitrate-water equilibration, Rapid Commun Mass Spectrom, 17, 1835-1846, 10.1002/rcm.1123, 2003.

Cape, J. N., Tang, Y. S., van Dijk, N., Love, L., Sutton, M. A., and Palmer, S. C.: Concentrations of ammonia and nitrogen dioxide at roadside verges, and their contribution to nitrogen deposition, Environ Pollut, 132, 469-478, 10.1016/j.envpol.2004.05.009, 2004.

Casciotti, K. L., Sigman, D. M., Hastings, M. G., Bohlke, J. K., and Hilkert, A.: Measurement of the oxygen isotopic composition of nitrate in seawater and freshwater using the denitrifier method, Analytical Chemistry, 74, 4905-4912, 10.1021/ac020113w, 2002.

Chang, Y., Liu, X., Deng, C., Dore, A. J., and Zhuang, G.: Source apportionment of atmospheric ammonia before, during, and after the 2014 APEC summit in Beijing using stable nitrogen isotope signatures, Atmospheric Chemistry and Physics, 16, 11635-11647, 10.5194/acp-16-11635-2016, 2016.

Chang, Y., Zhang, Y., Tian, C., Zhang, S., Ma, X., Cao, F., Liu, X., Zhang, W., Kuhn, T., and Lehmann, M. F.: Nitrogen isotope fractionation during gas-to-particle conversion of NOx to NO3- in the atmosphere – implications for isotope-based NOx source apportionment, Atmospheric Chemistry and Physics, 18, 11647-11661, 10.5194/acp-18-11647-2018, 2018.

Chen, C.-L., Chen, T.-Y., Hung, H.-M., Tsai, P.-W., Chou, C. C. K., and Chen, W.-N.: The influence of upslope fog on hygroscopicity and chemical composition of aerosols at a forest site in Taiwan, Atmospheric Environment, 246, 10.1016/j.atmosenv.2020.118150, 2021.

Chou, C. C.-K., Lee, C. T., Cheng, M. T., Yuan, C. S., Chen, S. J., Wu, Y. L., Hsu, W. C., Lung, S. C., Hsu, S. C., Lin, C. Y., and Liu, S. C.: Seasonal variation and spatial distribution of carbonaceous aerosols in Taiwan, Atmospheric Chemistry and

370   Physics, 10, 9563-9578, 10.5194/acp-10-9563-2010, 2010.

Chow, J. C., Watson, J. G., Crow, D., Lowenthal, D. H., and Merrifield, T.: Comparison of IMPROVE and NIOSH Carbon Measurements, Aerosol Science and Technology, 34, 23-34, 10.1080/02786820119073, 2001.

Coury, C. and Dillner, A. M.: A method to quantify organic functional groups and inorganic compounds in ambient aerosols using attenuated total reflectance FTIR spectroscopy and multivariate chemometric techniques, Atmospheric Environment,

375   42, 5923-5932, 10.1016/j.atmosenv.2008.03.026, 2008.

Evans, M. C., Campbell, S. W., Bhethanabotla, V., and Poor, N. D.: Effect of sea salt and calcium carbonate interactions with nitric acid on the direct dry deposition of nitrogen to Tampa Bay, Florida, Atmospheric Environment, 38, 4847-4858, 10.1016/j.atmosenv.2004.05.046, 2004.

Fan, M.-Y., Zhang, Y.-L., Lin, Y.-C., Chang, Y.-H., Cao, F., Zhang, W.-Q., Hu, Y.-B., Bao, M.-Y., Liu, X.-Y., Zhai, X.-Y.,

380   Lin, X., Zhao, Z.-Y., and Song, W.-H.: Isotope-based source apportionment of nitrogen-containing aerosols: A case study in an industrial city in China, Atmospheric Environment, 212, 96-105, 10.1016/j.atmosenv.2019.05.020, 2019.

Fan, M. Y., Zhang, Y. L., Lin, Y. C., Cao, F., Zhao, Z. Y., Sun, Y., Qiu, Y., Fu, P., and Wang, Y.: Changes of Emission Sources to Nitrate Aerosols in Beijing After the Clean Air Actions: Evidence From Dual Isotope Compositions, Journal of Geophysical Research: Atmospheres, 125, 10.1029/2019jd031998, 2020.

385   Fang, Y. T., Koba, K., Wang, X. M., Wen, D. Z., Li, J., Takebayashi, Y., Liu, X. Y., and Yoh, M.: Anthropogenic imprints on nitrogen and oxygen isotopic composition of precipitation nitrate in a nitrogen-polluted city in southern China, Atmospheric Chemistry and Physics, 11, 1313-1325, 10.5194/acp-11-1313-2011, 2011.

Felix, J. D. and Elliott, E. M.: Isotopic composition of passively collected nitrogen dioxide emissions: Vehicle, soil and livestock source signatures, Atmospheric Environment, 92, 359-366, 10.1016/j.atmosenv.2014.04.005, 2014.

390   Felix, J. D., Elliott, E. M., and Shaw, S. L.: Nitrogen isotopic composition of coal-fired power plant NOx: influence of emission controls and implications for global emission inventories, Environ Sci Technol, 46, 3528-3535, 10.1021/es203355v, 2012.

Felix, J. D., Elliott, E. M., Gish, T., Maghirang, R., Cambal, L., and Clougherty, J.: Examining the transport of ammonia emissions across landscapes using nitrogen isotope ratios, Atmospheric Environment, 95, 563-570, 10.1016/j.atmosenv.2014.06.061, 2014.

395   Gobel, A. R., Altieri, K. E., Peters, A. J., Hastings, M. G., and Sigman, D. M.: Insights into anthropogenic nitrogen deposition to the North Atlantic investigated using the isotopic composition of aerosol and rainwater nitrate, Geophysical Research Letters, 40, 5977-5982, 10.1002/2013gl058167, 2013.

Guha, T., Lin, C. T., Bhattacharya, S. K., Mahajan, A. S., Ou-Yang, C.-F., Lan, Y.-P., Hsu, S. C., and Liang, M.-C.: Isotopic ratios of nitrate in aerosol samples from Mt. Lulin, a high-altitude station in Central Taiwan, Atmospheric Environment, 154,

400   53-69, 10.1016/j.atmosenv.2017.01.036, 2017.

Hastings, M. G., Sigman, D. M., and Lipschultz, F.: Isotopic evidence for source changes of nitrate in rain at Bermuda, Journal of Geophysical Research: Atmospheres, 108, n/a-n/a, 10.1029/2003jd003789, 2003.

Hoffman, R. C., Laskin, A., and Finlayson-Pitts, B. J.: Sodium nitrate particles: physical and chemical properties during hydration and dehydration, and implications for aged sea salt aerosols, Journal of Aerosol Science, 35, 869-887, 10.1016/j.jaerosci.2004.02.003, 2004.

Hsieh, M.-K.: Effects of orographically induced low-level moisture convergence and inversion strength on upslope fog: a case study at Xitou, Graduate Institute of Atmospheric Sciences, National Taiwan University, Taipei, Taiwan, 10.6342/NTU201900872, 2019.

Huang, R.-T.: A study of aerosol hygroscopicity in Kinmen, Graduate Institute of Atmospheric Sciences, National Taiwan University, Taipei, Taiwan, 10.6342/NTU201603559, 2016.

Hung, H.-M., Hsu, C.-H., Lin, W.-T., and Chen, Y.-Q.: A case study of single hygroscopicity parameter and its link to the functional groups and phase transition for urban aerosols in Taipei City, Atmospheric Environment, 132, 240-248, 10.1016/j.atmosenv.2016.03.008, 2016.

Jacob, D. J.: Introduction to atmospheric chemistry, Princeton University Press1999.

Kawashima, H.: Seasonal trends of the stable nitrogen isotope ratio in particulate nitrogen compounds and their gaseous precursors in Akita, Japan, Tellus B, 71, 10.1080/16000889.2019.1627846, 2019.

Kim, H., Park, G.-H., Lee, S.-E., Kim, Y.-i., Lee, K., Kim, Y.-H., and Kim, T.-W.: Stable isotope ratio of atmospheric and seawater nitrate in the East Sea in the northwestern Pacific ocean, Marine Pollution Bulletin, 149, 10.1016/j.marpolbul.2019.110610, 2019.

Pan, Y., Tian, S., Liu, D., Fang, Y., Zhu, X., Gao, M., Gao, J., Michalski, G., and Wang, Y.: Isotopic evidence for enhanced fossil fuel sources of aerosol ammonium in the urban atmosphere, Environ Pollut, 238, 942-947, 10.1016/j.envpol.2018.03.038, 2018a.

Pan, Y., Tian, S., Liu, D., Fang, Y., Zhu, X., Zhang, Q., Zheng, B., Michalski, G., and Wang, Y.: Fossil Fuel Combustion-Related Emissions Dominate Atmospheric Ammonia Sources during Severe Haze Episodes: Evidence from (15)N-Stable Isotope in Size-Resolved Aerosol Ammonium, Environ Sci Technol, 50, 8049-8056, 10.1021/acs.est.6b00634, 2016.

Pan, Y., Tian, S., Liu, D., Fang, Y., Zhu, X., Gao, M., Wentworth, G. R., Michalski, G., Huang, X., and Wang, Y.: Source Apportionment of Aerosol Ammonium in an Ammonia-Rich Atmosphere: An Isotopic Study of Summer Clean and Hazy Days in Urban Beijing, Journal of Geophysical Research: Atmospheres, 123, 5681-5689, 10.1029/2017jd028095, 2018b.

Petters, M. D. and Kreidenweis, S. M.: A single parameter representation of hygroscopic growth and cloud condensation nucleus activity, Atmospheric Chemistry and Physics, 7, 1961-1971, 10.5194/acp-7-1961-2007, 2007.

Poschl, U.: Atmospheric aerosols: composition, transformation, climate and health effects, Angewandte Chemie International Edition, 44, 7520-7540, 10.1002/anie.200501122, 2005.

Savard, M. M., Cole, A., Smirnoff, A., and Vet, R.: δ15N values of atmospheric N species simultaneously collected using sector-based samplers distant from sources – Isotopic inheritance and fractionation, Atmospheric Environment, 162, 11-22, 10.1016/j.atmosenv.2017.05.010, 2017.

Savarino, J., Kaiser, J., Morin, S., Sigman, D. M., and Thiemens, M. H.: Nitrogen and oxygen isotopic constraints on the origin of atmospheric nitrate in coastal Antarctica, Atmospheric Chemistry and Physics, 7, 1925-1945, 10.5194/acp-7-1925-2007, 2007.

Seinfeld, J. H. and Pandis, S. N.: Atmospheric Chemistry and Physics: From Air Pollution to Climate Change, 2nd, John Wiley & Sons, Inc.2006.

Sigman, D. M., Casciotti, K. L., Andreani, M., Barford, C., Galanter, M., and Böhlke, J. K.: A Bacterial Method for the Nitrogen Isotopic Analysis of Nitrate in Seawater and Freshwater, Analytical Chemistry, 73, 4145-4153, 10.1021/ac010088e, 2001.

Stock, B. C., Jackson, A. L., Ward, E. J., Parnell, A. C., Phillips, D. L., and Semmens, B. X.: Analyzing mixing systems using a new generation of Bayesian tracer mixing models, PeerJ, 6, e5096, 10.7717/peerj.5096, 2018.

Sun, X., Zong, Z., Wang, K., Li, B., Fu, D., Shi, X., Tang, B., Lu, L., Thapa, S., Qi, H., and Tian, C.: The importance of coal combustion and heterogeneous reaction for atmospheric nitrate pollution in a cold metropolis in China: Insights from isotope fractionation and Bayesian mixing model, Atmospheric Environment, 243, 10.1016/j.atmosenv.2020.117730, 2020.

Walters, W. W. and Michalski, G.: Theoretical calculation of nitrogen isotope equilibrium exchange fractionation factors for various NO y molecules, Geochimica et Cosmochimica Acta, 164, 284-297, 10.1016/j.gca.2015.05.029, 2015.

Walters, W. W., Chai, J., and Hastings, M. G.: Theoretical Phase Resolved Ammonia–Ammonium Nitrogen Equilibrium Isotope Exchange Fractionations: Applications for Tracking Atmospheric Ammonia Gas-to-Particle Conversion, ACS Earth and Space Chemistry, 3, 79-89, 10.1021/acsearthspacechem.8b00140, 2018.

Walters, W. W., Tharp, B. D., Fang, H., Kozak, B. J., and Michalski, G.: Nitrogen Isotope Composition of Thermally Produced NOx from Various Fossil-Fuel Combustion Sources, Environ Sci Technol, 49, 11363-11371, 10.1021/acs.est.5b02769, 2015.

Wankel, S. D., Chen, Y., Kendall, C., Post, A. F., and Paytan, A.: Sources of aerosol nitrate to the Gulf of Aqaba: Evidence from δ15N and δ18O of nitrate and trace metal chemistry, Marine Chemistry, 120, 90-99, 10.1016/j.marchem.2009.01.013, 2010.

Weigand, M. A., Foriel, J., Barnett, B., Oleynik, S., and Sigman, D. M.: Updates to instrumentation and protocols for isotopic analysis of nitrate by the denitrifier method, Rapid Commun Mass Spectrom, 30, 1365-1383, 10.1002/rcm.7570, 2016.

Wu, L., Yue, S., Shi, Z., Hu, W., Chen, J., Ren, H., Deng, J., Ren, L., Fang, Y., Yan, H., Li, W., Harrison, R. M., and Fu, P.: Source forensics of inorganic and organic nitrogen using δ15N for tropospheric aerosols over Mt. Tai, npj Climate and Atmospheric Science, 4, 10.1038/s41612-021-00163-0, 2021.

Zhang, Z., Zeng, Y., Zheng, N., Luo, L., Xiao, H., and Xiao, H.: Fossil fuel-related emissions were the major source of NH3 pollution in urban cities of northern China in the autumn of 2017, Environ Pollut, 256, 113428, 10.1016/j.envpol.2019.113428, 2020.

Tables

Table 1. The average concentration of collected PM_{10} using IR functional group analysis under different weather conditions. (mean, [min, max] at the unit of $\mu g/m^3$)

	Overall	non-foggy daytime	foggy daytime	non-foggy nighttime	foggy nighttime
NH_4^+	0.98, [0.15, 3.31]	1.00	2.48	0.56	1.12
NO_3^-	0.25, [0.00, 1.51]	0.25	0.92	0.04	0.34
SO_4^{2-}	5.16, [0.62, 12.97]	5.62	10.14	3.58	5.01
BC	0.81, [0.48, 1.46]	0.95	1.25	0.59	0.71

Table 2. Aerosol δ^{15}N values of different sources used in this study (Savard et al., 2017).

NH$_4^+$ source	NH$_4^+$ δ^{15}N (mean ± SD)	NO$_3^-$ source	NO$_3^-$ δ^{15}N (mean ± SD)
CFPP	3.4 ± 10.4	CFPP	6.1 ± 2.0
traffic	17.1 ± 9.1	urban	5.7 ± 2.0
chemical and metal industries	11.0 ± 2.4	chemical and metal industries	1.0 ± 4.7
fertilizers plus oil	16.3	fertilizers plus oil	10.8
feedlots	27.7 ± 7.0		

475

Table 3. Mass-weighted isotope value (‰) and probable single source under distinct weather circumstances.

	Non-foggy daytime	Foggy daytime	Non-foggy nighttime	Foggy nighttime
$\delta^{15}N$ of NH_4^+ (probable sources)	13.20 (CFPP, traffic, industries)	15.52 (traffic)	9.30 (CFPP, traffic, industries)	13.33 (CFPP, traffic, industries)
$\delta^{15}N$ of $PM_1\text{-}NO_3^-$ (probable sources)	-	1.70 (industries)	-	1.46 (industries)
$\delta^{15}N$ of $PM_{1\text{-}10}\text{-}NO_3^-$ (probable sources)	2.72 (industries)	3.98 (urban, industries)	1.85 (industries)	-
$\delta^{18}O$ of $PM_1\text{-}NO_3^-$	-	70.48	-	79.81
$\delta^{18}O$ of $PM_{1\text{-}10}\text{-}NO_3^-$	70.05	71.62	74.82	-

Table 4. The posterior probabilities of aerosol sources inferred by MixSIAR (starred for the mean posterior probability greater than 20%.)

Weather condition (sample size, n)	NH$_4^+$ sources and posterior probabilities (Mean ± SD, %)				
	CFPP	industries	feedlots	fertilizers	traffic
all cases (10)	25.7 ± 15.1*	32.5 ± 22.0*	9.2 ± 8.2	17.7 ± 14.3	15.0 ± 13.5
non-foggy day (3)	19.0 ± 14.6	28.5 ± 20.0*	13.8 ± 12.0	22.1 ± 17.4*	16.6 ± 14.1
foggy day (2)	13.9 ± 12.5	24.2 ± 17.9*	17.0 ± 13.6	27.2 ± 20.9*	17.7 ± 14.8
non-foggy night (4)	21.0 ± 14.7*	32.3 ± 21.2*	10.6 ± 9.8	20.5 ± 16.4*	15.5 ± 13.4
foggy night (1)	19.1 ± 15.0	23.1 ± 17.9*	17.3 ± 14.3	20.5 ± 17.0*	20.0 ± 15.9*

	PM$_{1-10}$-NO$_3^-$ sources			
	CFPP	industries	fertilizers	urban
all cases (5)	27.2 ± 19.3*	30.7 ± 17.8*	13.9 ± 12.2	28.2 ± 19.8*
non-foggy day (2)	27.8 ± 19.7*	25.2 ± 18.0*	19.7 ± 15.6	27.4 ± 20.3*
foggy day (2)	28.0 ± 19.9*	25.3 ± 17.3*	19.2 ± 15.4	27.6 ± 19.4*
non-foggy night (1)	26.5 ± 20.5*	27.2 ± 19.6*	19.8 ± 16.2	26.5 ± 20.0*

	PM$_1$-NO$_3^-$ sources			
	CFPP	industries	fertilizers	urban
all cases (3)	23.8 ± 18.2*	36.5 ± 21.0*	14.6 ± 13.3	25.1 ± 19.2*
foggy day (2)	26.6 ± 19.9*	30.0 ± 19.4*	16.6 ± 14.8	26.7 ± 19.7*
foggy night (1)	27.4 ± 19.9*	26.9 ± 19.3*	19.1 ± 15.8	26.6 ± 19.7*

Figures
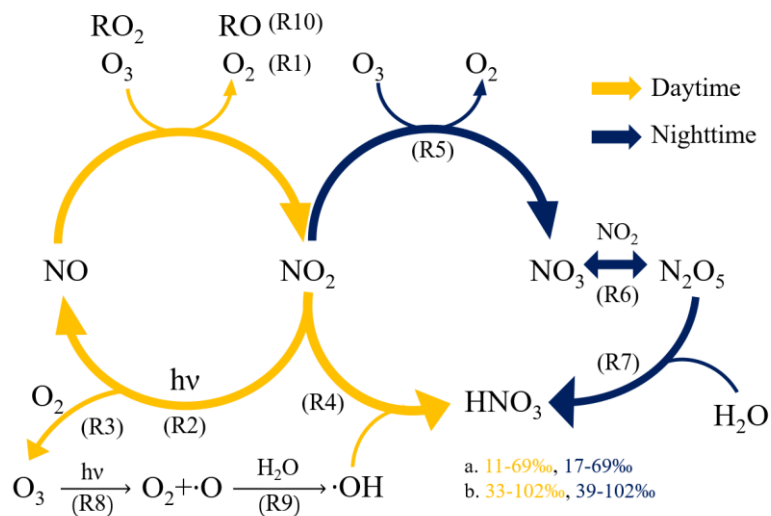
Figure 1: The formation pathway of nitric acid to form aerosol nitrate during daytime (orange color) and nighttime (blue color) with the predicted $\delta^{18}O$ range of NO_3^- based on (a) freshly emitted NO and (b) NO cycled from NO_2, fully reacted with O_3 detail can be found in Figures S6 and S7).

485
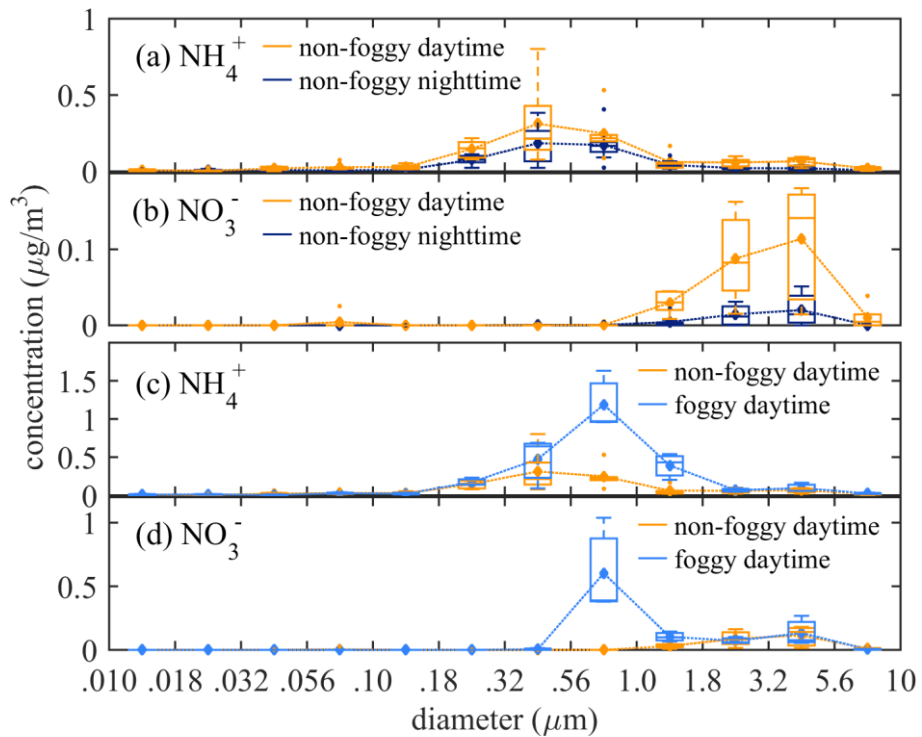
Figure 2: The statistical box plot of concentrations as a function of size bin at non-foggy daytime and nighttime for (a) NH₄⁺, and (b) NO₃⁻, and at foggy and non-foggy daytime for (c) NH₄⁺ and (d) NO₃⁻. (diamond: mean value; outliers: < 1ˢᵗ quartile Q1-1.5 interquartile range (IQR) or > 3ʳᵈ quartile Q3+1.5 IQR).
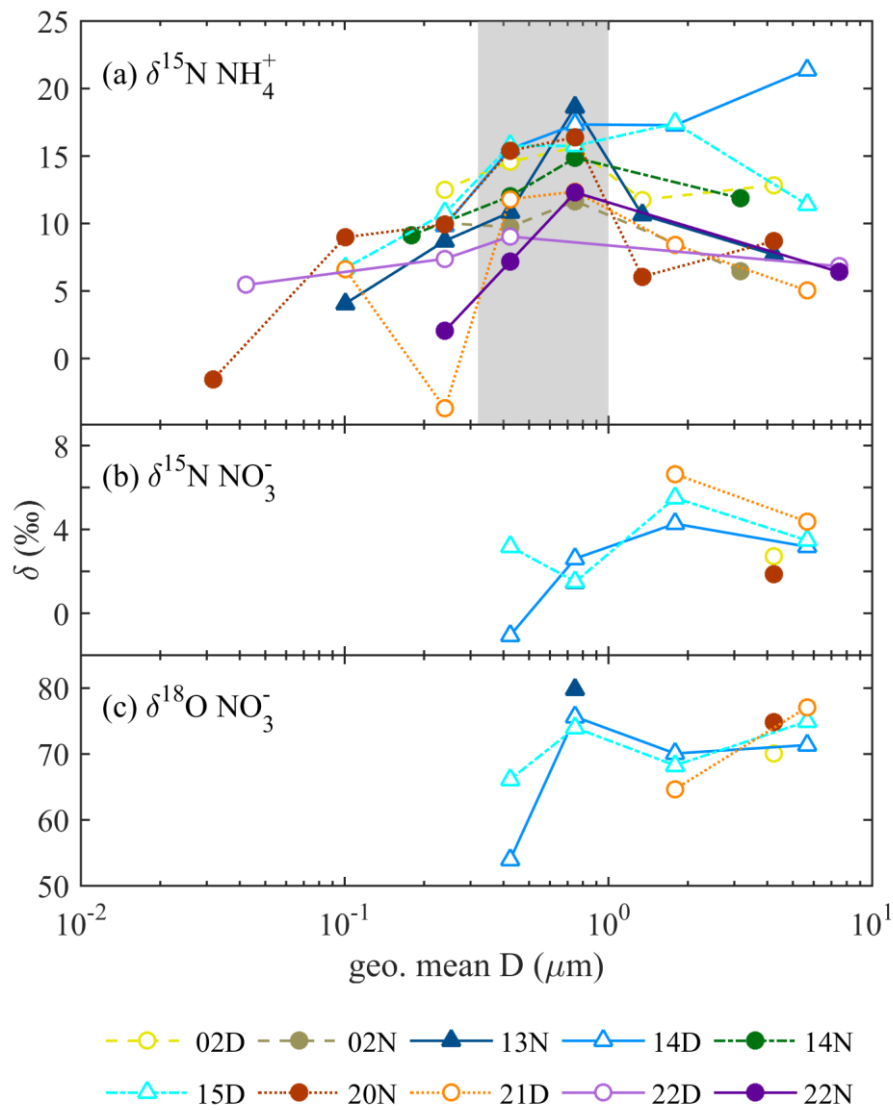
Figure 3: The isotope values as a function of collected aerosol geometric mean diameter (D) (a) $\delta^{15}N\ NH_4^+$, (b) $\delta^{15}N\ NO_3^-$, and (c) $\delta^{18}O\ NO_3^-$. Symbol conditions: hollow for daytime, filled for nighttime, and triangle for foggy events.
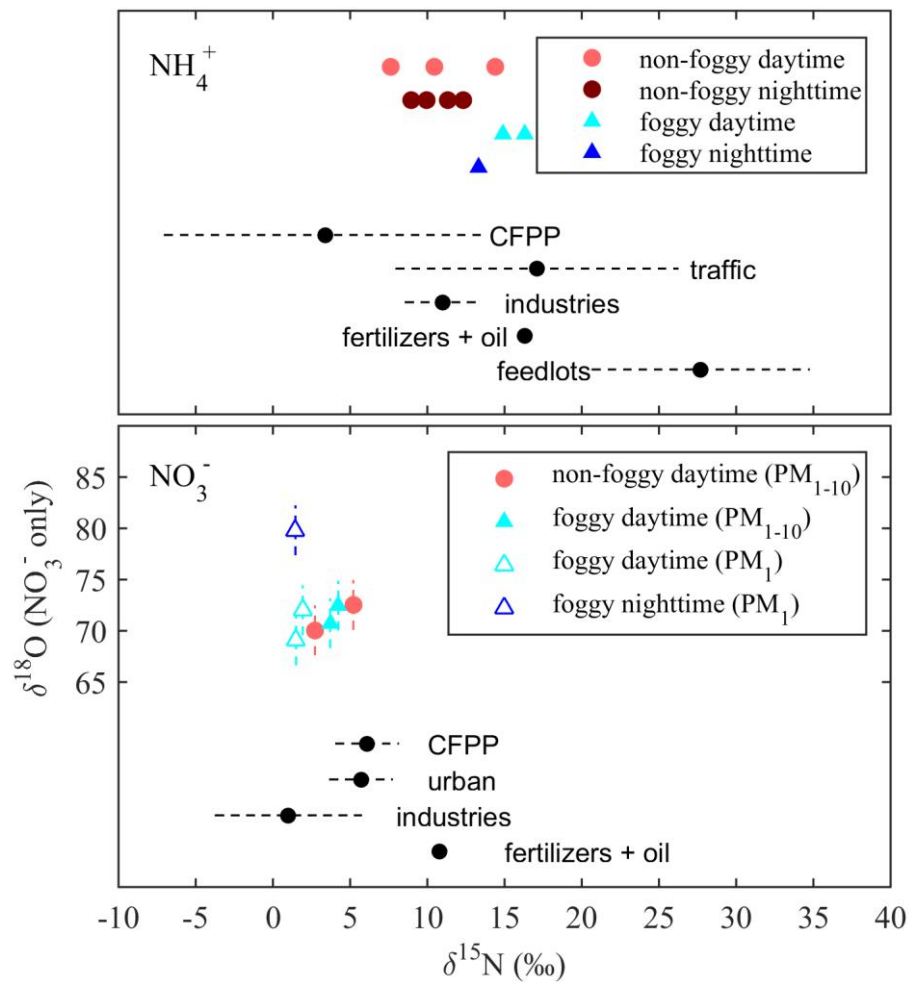
Figure 4: Comparison between the period mass-averaged isotope values ($\delta^{15}N$ and $\delta^{18}O$) and the mean $\delta^{15}N$ value (black dots) by Savard et al. (2017) for different sources. The dashed lines are the standard deviation of the measurements. The batch SD of international standards' duplicates was 0.04 - 0.11‰ for $\delta^{15}N$ (not observable in this figure), and 2.20 - 2.33‰ for $\delta^{18}O$ as shown at each data point.